UKACC International Conference on Control 2012
Cardiff, UK, 3-5 September 2012

Design and Control of Novel Tri-rotor UAV

Mohamed Kara Mohamed
School of Electrical and
Electronic Engineering
The University of Manchester
Manchester, UK, M13 9PL
Email: Mohamed.KaraMohamed@postgrad.manchester.ac.uk

Alexander Lanzon
School of Electrical and
Electronic Engineering
The University of Manchester
Manchester, UK, M13 9PL
Email: Alexander.Lanzon@manchester.ac.uk

***Abstract*—Tri-rotor UAVs are more efficient compared to quadrotors in regard to the size and power requirement, yet, tri-rotor UAVs are more challenging in terms of control and stability. In this paper, we propose the design and control of a novel tri-rotor UAV. The proposed platform is designed to achieve six degree of freedom using a thrust vectoring technique with the highest level of flexibility, manoeuvrability and minimum requirement of power. The proposed tri-rotor has a triangular shape of three arms where at the end of each arm, a fixed pitch propeller is driven by a DC motor. A tilting mechanism is employed to tilt the motor-propeller assembly and produce thrust in the desired direction. The three propellers can be tilted independently to achieve full authority of torque and force vectoring. A feedback linearization associated with $\mathscr{H}_\infty$ loop shaping design is used to synthesize a controller for the system. The results are verified via simulation.**

I. Background and Motivation

In recent decades, Unmanned Aerial Vehicles (UAVs) have attracted growing attention in research due to their wide applications and large potential [1]. Aiming for more efficiency in term of size, autonomy, maneuverability and other factors, various conventional and non-conventional structure designs and configurations of UAV systems are proposed, see [2] and the literature therein. One such design that attracts increasing interest is the vertical-take-off-and-landing (VTOL) tri-rotor configuration.

Tri-rotor vehicles are systems with a three rotors arrangement. This configuration has been proposed as less-expensive with more flexibility and great agility [3], [4]. Compared to quadrotors, tri-rotor UAVs are smaller in size, less complex, less costly and have longer flight time due to the reduction in number of motors [5], which makes tri-rotor vehicles ideal for deployment in various research projects and missions [6].

On another perspective, thrust vectoring has been used in designs to maximize the capability of UAVs [7]. Thrust vectoring is of significant benefit in some applications to arbitrarily orient the vehicle body with respect to the vehicle acceleration vector [8]. In addition, thrust vectoring mechanism is used to give UAVs the capability of taking-off and landing in very narrow areas [9]. In small aircrafts and UAVs, a simple technique of tilt-rotor mechanism can be used to obtain thrust vectoring, where propulsion units are inclined in certain angles using an additional control motor to get the desired thrust in different directions. In general, tilt-rotor mechanism is used in tri-rotor systems to control the horizontal forces and yaw torque of the vehicle. Typically, one rotor only, referred to as the tail rotor, has the ability to tilt to control the yaw moment, see for example [6].

Dynamics of tri-rotor vehicles are highly coupled and nonlinear, which makes the control design of these vehicles the key for successful flight and operations [5]. Compared to quadrotor systems, the yaw control of tri-rotor systems is a further challenge due to the asymmetric configuration of the system. For instance, the reactive yaw moments in quadrotor systems is decoupled from pitch and roll moments which simplifies the yaw control design in such systems. In contrary, pitch, roll and yaw moments are highly coupled in tri-rotor systems. Moreover, attitude control of these vehicles is more challenging compared to quadrotor systems due to gyroscopic and Coriolis terms. In [5], the authors propose a tri-rotor system of which the control design is implemented by four loops for attitude control and guidance. This control design is complicated with coupling between attitude and position control loops and high computation load. The authors in [3] propose a tri rotor configuration in which all rotors of the system tilt simultaneously to the same angle to attain yaw control. The control design considers only the attitude stabilization and neglects the trajectory tracking. The control algorithm in [4] is based on nest saturation for decoupled channels where the configuration of the vehicle makes the separate control of attitude and position possible. The control design of the tri-rotor UAV proposed in [10] discusses only the hovering position. In [11], the attitude of the proposed tri-rotor UAV is controlled by using differential thrust concept between the rotors. The control system design in [12] controls the yaw angle of the proposed tri-rotor UAV by differentially tilting the two main rotors in the plane of symmetry while a fixed up-right propeller is used at the tail to control the pitch moment.

Few researchers have identified the structure of tri-rotor UAV combined with full independent tilt-rotor capability. In this paper, we propose a novel tri-rotor platform, herein referred to as the Tri-rotor UAV, and then we discuss the design and control of the proposed system. The proposed vehicle can achieve full authority of torque and force vectoring by employing three rotors and three servos for tilt-rotor mechanism. This structure gives the vehicle high level of maneuverability and

978-1-4673-1558-6/12/$31.00 ©2012 IEEE

flexibility for translational motion as well as attitude control.

The rest of the paper is organized as follows. In Section II, a functional description of the vehicle and its design is discussed. A mathematical model that captures the dynamics of the UAV and govern the behaviour of the system is derived in Section III. The control system design is presented in Section IV and the simulation results is shown in Section V. The paper ends by conclusion in Section VI.

II. System Structure and Design

The structure of the proposed Tri-rotor UAV is depicted in Figure 1. The vehicle has a triangular structure of three arms and at the end of each arm, a force generating unit is mounted to produce part of the required controlling force/torque. All three arms are identical of length l and the three force generating units are also identical. Each force generating unit consists of a fixed pitch propeller driven by a Brushless DC (BLDC) motor to generate thrust. The three motors can be powered by a single battery pack or three separate packs located at the center of the body. The propeller-motor assembly is attached

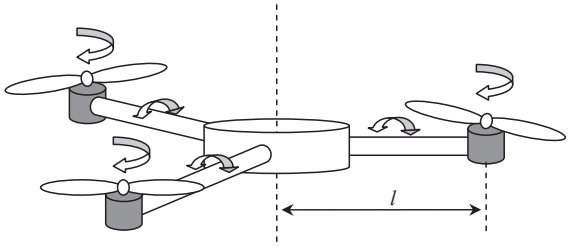

Figure 1. The design of the Tri-rotor UAV (3D view).

to the body arm via a servo motor that can rotate in a vertical plane to tilt the propeller-motor assembly with an angle α_{s_i} in the range $\frac{-\pi}{2} \leq \alpha_{s_i} \leq \frac{\pi}{2}$, $i = 1,2,3$ to produce a horizontal component of the generated force, see Figure 2. All three propellers can be tilted independently to give full authority of thrust vectoring. The system has six degree of freedom in which all movements can be achieved independently and directly by changing the norm of the generated thrust and the tilting angles. This configuration enables the vehicle body to stay aligned in the required direction regardless of the movement the UAV makes.

III. Mathematical Modeling

To develop the dynamic model of the UAV, we consider the following right hand coordinate systems shown in Figure 3:
e: the generalized earth coordinate system of axes X_e, Y_e, Z_e.
b: the body fixed coordinate system in which the origin coincides with the centre of mass of the UAV. The axes of frame b are denoted by X_b, Y_b, Z_b. In addition, we choose three right hand coordinate systems l_i of axes X_{l_i}, Y_{l_i}, Z_{l_i} with $i = 1,2,3$. These coordinate systems are termed as local coordinate systems and located at the locations of the three propellers, see Figure 4. The origin of each local coordinate

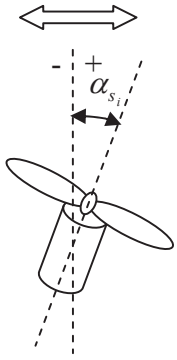

Figure 2. Front view of one arm.

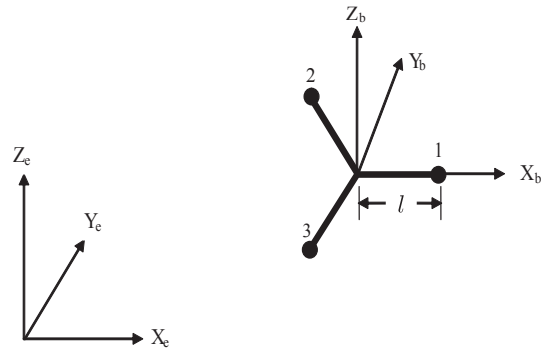

Figure 3. Coordinate systems used to develop the UAV dynamic model.

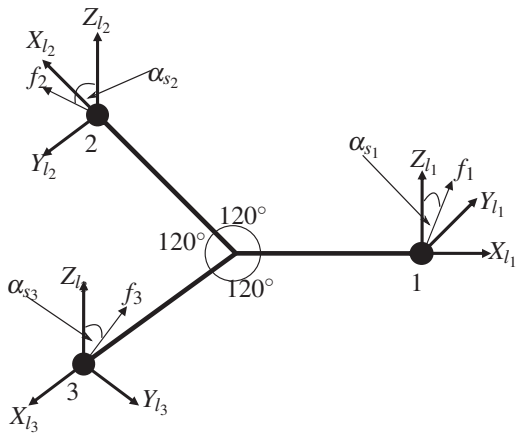

Figure 4. Local coordinate systems at the three propulsion units.

system coincides with the joining point between the UAV arm and the propulsion unit where X_{l_i} is extended outside the i^{th} arm of the UAV and Z_{l_i} is along the BLDC motor shaft axis when the tilting angle is zero.

The rotation matrices between the defined coordinate systems are denoted by:
$\boldsymbol{R}_e^b$: the rotational matrix from frame e to frame b.
$\boldsymbol{R}_{l_i}^b$: the rotational matrix from coordinate system l_i to coordinate system b, $i = 1,2,3$.

In the sequel, we use superscript b, e and l_i to denote

the coordinate system in which vectors are expressed. The subscript i refers to the i^{th} BLDC motor, servo motor or propeller as applies where $i = 1,2,3$.

In order to obtain the dynamic equations of the UAV, we need to obtain forces and torques acting on the vehicle. We assume very fast actuators and therefore the dynamics of the actuators are neglected.

Forces

There are two main forces acting on the UAV which are the propulsive force and the gravitational force.

The propulsive force: The total propulsive force $F_{p\Sigma}$ is equal to the algebraic sum of the three individual propulsive forces generated from propellers. The individual propulsive forces of the three propellers expressed in the local coordinate systems can be written as [13]:

$$F_{p_i}^{l_i} = \begin{bmatrix} 0 \\ k_f \omega_{m_i}^2 \sin(\alpha_{s_i}) \\ k_f \omega_{m_i}^2 \cos(\alpha_{s_i}) \end{bmatrix}, \; i = 1,2,3. \tag{1}$$

where k_f is the thrust to speed constant of the propeller and it is identical for all three propellers, ω_{m_i} is the rotational speed of the i^{th} BLDC motor (we assume direct driving of the propeller, i.e., the rotational speed of the motor equals the rotational speed of the propeller) and α_{s_i} is the tilting angle of the i^{th} Servo motor.

In the body coordinate system, the individual propulsive forces are given by:

$$F_{p_i}^b = \boldsymbol{R}_{l_i}^b F_{P_i}^{l_i}, \; i = 1,2,3. \tag{2}$$

From Figure 4, we can obtain the rotation matrices from the local coordinate systems l_1, l_2 and l_3 to the body coordinate system b as:

$$\boldsymbol{R}_{l_1}^b = \begin{bmatrix} 1 & 0 & 0 \\ 0 & 1 & 0 \\ 0 & 0 & 1 \end{bmatrix}, \boldsymbol{R}_{l_2}^b = \begin{bmatrix} -\frac{1}{2} & -\frac{\sqrt{3}}{2} & 0 \\ \frac{\sqrt{3}}{2} & -\frac{1}{2} & 0 \\ 0 & 0 & 1 \end{bmatrix}, \boldsymbol{R}_{l_3}^b = \begin{bmatrix} -\frac{1}{2} & \frac{\sqrt{3}}{2} & 0 \\ -\frac{\sqrt{3}}{2} & -\frac{1}{2} & 0 \\ 0 & 0 & 1 \end{bmatrix}. \tag{3}$$

Using Eq.(3), the total propulsive force is:

$$F_{p\Sigma}^b = F_{p_1}^b + F_{p_2}^b + F_{p_3}^b \tag{4}$$

$$= k_f \boldsymbol{H}_f \rho. \tag{5}$$

where

$$\boldsymbol{H}_f = \begin{bmatrix} 0 & -\frac{\sqrt{3}}{2} & \frac{\sqrt{3}}{2} & 0 & 0 & 0 \\ 1 & -\frac{1}{2} & -\frac{1}{2} & 0 & 0 & 0 \\ 0 & 0 & 0 & 1 & 1 & 1 \end{bmatrix}, \rho = \begin{bmatrix} \omega_{m_1}^2 \sin(\alpha_{s_1}) \\ \omega_{m_2}^2 \sin(\alpha_{s_2}) \\ \omega_{m_3}^2 \sin(\alpha_{s_3}) \\ \omega_{m_1}^2 \cos(\alpha_{s_1}) \\ \omega_{m_2}^2 \cos(\alpha_{s_2}) \\ \omega_{m_3}^2 \cos(\alpha_{s_3}) \end{bmatrix}. \tag{6}$$

The gravity force: The gravitational force in the generalized earth coordinate system is given as:

$$F_g^e = \begin{bmatrix} 0 \\ 0 \\ -gM_{tot} \end{bmatrix}. \tag{7}$$

where g is the gravitational acceleration and M_{tot} is the total mass of the UAV.

In the body coordinate system, we have:

$$F_g^b = \boldsymbol{R}_e^b F_g^e. \tag{8}$$

Using the general notation of rotation angles for the UAV attitude: Roll ϕ_v, Pitch θ_v and Yaw ψ_v around the axes X_e, Y_e and Z_e respectively, the gravity force in the body system is given by:

$$F_g^b = gM_{tot}H_g \tag{9}$$

where

$$H_g = \begin{bmatrix} \sin(\theta_v) \\ -\sin(\phi_v)\cos(\theta_v) \\ -\cos(\phi_v)\cos(\theta_v) \end{bmatrix}. \tag{10}$$

Now, the total force acting on the UAV and expressed in the body coordinate system is:

$$F^b = F_{p\Sigma}^b + F_g^b \tag{11}$$

$$= k_f \boldsymbol{H}_f \rho + gM_{tot}H_g. \tag{12}$$

Torques

The two main torques acting on the UAV are the propulsive torque and the drag torque.

The propulsive torque: The propulsive torque is the torque resulting from the generated propulsive force around the center of mass of the vehicle. For the case of the Tri-rotor UAV, we have three identical arms and then the components of the propulsive torque are:

$$\tau_{p_i}^b = \vec{l}_i^b \times F_{p_i}^b, \; i = 1,2,3. \tag{13}$$

where $\vec{l}_i^b$ is the vector of the i^{th} arm between the center of mass of the UAV and the propulsion unit expressed in the body coordinate system. $F_{b_i}^b$ is obtained from Eq. (2).

Now, the total propulsive torque expressed in the body coordinate system is:

$$\tau_{p\Sigma}^b = \tau_{p_1}^b + \tau_{p_2}^b + \tau_{p_3}^b \tag{14}$$

$$= k_f \boldsymbol{H}_t \rho \tag{15}$$

where

$$\boldsymbol{H}_t = l \begin{bmatrix} 0 & 0 & 0 & 0 & \frac{\sqrt{3}}{2} & -\frac{\sqrt{3}}{2} \\ 0 & 0 & 0 & -1 & \frac{1}{2} & \frac{1}{2} \\ 1 & 1 & 1 & 0 & 0 & 0 \end{bmatrix}, \tag{16}$$

l is the length of the vehicle's arm measured between the center of mass of the UAV and the propulsion unit (identical for the three arms) and ρ is defined in Eq. (6).

The drag torque: The drag torque is defined as the torque resulting from the aerodynamic drag forces exerted by the ambient fluid (air) on the propeller. Drag torque is in the opposite direction to the direction of rotation. In our case, the resulting drag torque on the i^{th} propeller can be approximated by $\tau_{d_i} = -k_t \omega_{m_i}^2$ [14], where k_t is the drag torque to speed constant resulting from the rotation of the propeller and ω_{m_i} is the rotational speed of the motor (we consider the BLDC motors drives the propeller directly). In the local coordinate systems l_i, the drag torque can be written as:

$$\tau_{d_i}^{l_i} = \begin{bmatrix} 0 \\ -k_t \omega_{m_i}^2 \sin(\alpha_{s_i}) \\ -k_t \omega_{m_i}^2 \cos(\alpha_{s_i}) \end{bmatrix}, \; i = 1,2,3. \tag{17}$$

In the body coordinate system, the individual drag torques can be represented as:

$$\tau_{d_i}^b = \boldsymbol{R}_{l_i}^b \tau_{d_i}^{l_i}, \tag{18}$$

Using definitions (3), the total drag torque in the body system is given by:

$$\tau_{d_\Sigma}^b = \tau_{d_1}^b + \tau_{d_2}^b + \tau_{d_3}^b \tag{19}$$

$$= -k_t \boldsymbol{H}_f \rho, \tag{20}$$

where $\boldsymbol{H}_f$ and ρ are defined in (6).

Now, the total torque acting on the Tri-rotor and expressed in the body coordinate system is:

$$\tau^b = \tau_{p_\Sigma}^b + \tau_{d_\Sigma}^b \tag{21}$$

$$= \left(k_f \boldsymbol{H}_t - k_t \boldsymbol{H}_f\right) \rho. \tag{22}$$

Dynamic Model: Assuming that the Tri-rotor UAV is a rigid body of fixed mass, the vehicle's motion can be described by the Newton-Euler second's law in the body coordinate system as:
for translational motion: $F^b = M_{tot}\left(\dot{\upsilon}_v^b + \boldsymbol{S}(\omega_v^b)\upsilon_v^b\right)$,
for rotational motion: $\tau^b = \boldsymbol{I}_v^b \dot{\omega}_v^b + \boldsymbol{S}(\omega_v^b)\boldsymbol{I}_v^b \omega_v^b$,
where υ_v^b is the translational velocity of the UAV, ω_v^b is the angular velocity of the UAV, $\boldsymbol{S}(\omega^b)$ is the skew matrix of the vector ω_v^b and $\boldsymbol{I}_v^b$ is the inertia matrix of the UAV all with respect to the fixed body coordinate system. Assuming no mass change over time, $\boldsymbol{I}_v^b$ is fixed.

Now, Substituting F^b and τ^b from (12) and (22) gives:

$$k_f \boldsymbol{H}_f \rho + g M_{tot} H_g = M_{tot}\left(\dot{\upsilon}_v^b + \boldsymbol{S}(\omega_v^b)\upsilon_v^b\right) \tag{23}$$

$$(k_f \boldsymbol{H}_t - k_t \boldsymbol{H}_f)\rho = \boldsymbol{I}_v^b \dot{\omega}_v^b + \boldsymbol{S}(\omega_v^b)\boldsymbol{I}_v^b \omega_v^b \tag{24}$$

Let η_v and λ_v^e be the attitude vector and the position vector of the UAV related to the earth coordinate system and defined as:

$$\eta_v = \begin{bmatrix} \phi_v & \theta_v & \psi_v \end{bmatrix}^T, \; \lambda_v^e = \begin{bmatrix} x_v & y_v & z_v \end{bmatrix}^T.$$

To fully describe the dynamic equations of the UAV, we have the following relations from [15]:

$$\dot{\eta}_v = \boldsymbol{\Psi}\omega_v^b \;, \; \dot{\lambda}_v^e = (\boldsymbol{R}_e^b)^{-1}\upsilon_v^b$$

where $\boldsymbol{\Psi}$ is the rotational matrix between the angular velocity expressed in the body coordinate system ω_v^b and the angular velocity in the earth coordinate system $\dot{\eta}_v$. $\boldsymbol{\Psi}$ is given in [15] as:

$$\boldsymbol{\Psi} = \begin{bmatrix} 1 & \sin(\phi_v)\tan(\theta_v) & \cos(\phi_v)\tan(\theta_v) \\ 0 & \cos(\phi_v) & -\sin(\phi_v) \\ 0 & \sin(\phi_v)\sec(\theta_v) & \cos(\phi_v)\sec(\theta_v) \end{bmatrix}, \; \frac{-\pi}{2} < \theta_v < \frac{\pi}{2}. \tag{25}$$

From the properties of the rotation matrix we have $(\boldsymbol{R}_e^b)^{-1} = \boldsymbol{R}_b^e$, where $\boldsymbol{R}_b^e$ is the rotation matrix from the body coordinate system b to the earth coordinate system e.

Finally, the dynamic model of the UAV can be written as:

$$\dot{\upsilon}^b{}_v = gH_g - \boldsymbol{S}(\omega_v^b)\upsilon_v^b + \frac{k_f}{M_{tot}}\boldsymbol{H}_f \rho \tag{26}$$

$$\dot{\omega}^b{}_v = -(\boldsymbol{I}_v^b)^{-1}\boldsymbol{S}(\omega_v^b)\boldsymbol{I}_v^b \omega_v^b + (\boldsymbol{I}_v^b)^{-1}(k_f \boldsymbol{H}_t - k_t \boldsymbol{H}_f)\rho \tag{27}$$

$$\dot{\eta}_v = \boldsymbol{\Psi}\omega_v^b \tag{28}$$

$$\dot{\lambda}_v^e = \boldsymbol{R}_b^e \upsilon_v^b \tag{29}$$

This model of the UAV is written in the compact form in which every state variable is a vector of three components, i.e., $x \in \mathbb{R}^{12}$, where:

$$\upsilon_v^b = \begin{bmatrix} u \\ v \\ w \end{bmatrix}, \; \omega_v^b = \begin{bmatrix} p \\ q \\ r \end{bmatrix}, \; \eta_v = \begin{bmatrix} \phi_v \\ \theta_v \\ \psi_v \end{bmatrix}, \; \lambda_v^e = \begin{bmatrix} x_v \\ y_v \\ z_v \end{bmatrix}.$$

Equations (26) - (29) show a nonlinear model with coupling between the translational and rotational dynamics of the UAV. Moreover, there is coupling between inputs and output channels in which all inputs act on all outputs. The system coupling along with the nonlinearity of the system makes the control design of the proposed Tri-rotor UAV a real challenge compared with other UAV configurations. On the other hand, if we consider the control problem of the UAV to be position tracking with attitude regulating, then the system is square in which we have six actuators (three BLDC motor speeds and three servo angles) and six outputs (3D position and three attitude angles). This highlights the positive aspect of the proposed configuration in terms of controller design compared to other UAV systems that are in general under-actuated systems such as quadrotors.

IV. Control System Design

In this section we consider the control design for the proposed Tri-rotor UAV using input-output feedback linearisation and $\mathscr{H}_\infty$ Loop Shaping Design Procedure (LSDP). The control design of the system can be seen as a tracking problem for the position and attitude of the vehicle via the speed of the BLDC motors and the angles of the servo motors. In this case, the system is fully actuated having six outputs and six inputs. The proposed control algorithm is a centralized $\mathscr{H}_\infty$ controller that stabilizes and tracks simultaneously all outputs, i.e., 3D position and three attitude angles. The motivation behind such a centralized control design is to synthesize a robust controller that can compensate for any unmodeled coupling between channels and attenuate cross-coupling noises and disturbances. Moreover, the implementation of such a design is simple via a single feedback loop structure.

In the sequel and for simplicity of expression, the superscript b and e as well as the subscript v are not written unless it is necessary to avoid ambiguity. We consider the vector ρ as the input vector for the UAV system, i.e., $u = \rho$, and we have the output as $y = \begin{bmatrix} \eta & \lambda \end{bmatrix}^T$

To implement input-output feedback linearization, we have:

$$\dot{y} = y^{(1)} = \begin{bmatrix} \dot{\eta} \\ \dot{\lambda} \end{bmatrix} = \begin{bmatrix} \boldsymbol{\Psi}\omega \\ \boldsymbol{R}_b^e \upsilon_v \end{bmatrix} \tag{30}$$

and

$$\ddot{y} = y^{(2)} = \begin{bmatrix} \dot{\boldsymbol{\Psi}}\omega + \boldsymbol{\Psi}\dot{\omega} \\ (\dot{\boldsymbol{R}}_b^e)\upsilon + \boldsymbol{R}_b^e\dot{\upsilon} \end{bmatrix} \tag{31}$$

From the general properties of the rotation matrix, we have $\dot{\boldsymbol{R}}_b^e = \boldsymbol{R}_b^e \boldsymbol{S}(\omega^b)$ [16], and then we write:

$$\begin{aligned} y^{(2)} &= \begin{bmatrix} \dot{\boldsymbol{\Psi}}\omega + \boldsymbol{\Psi}(-\boldsymbol{I}^{-1}\boldsymbol{S}(\omega)\boldsymbol{I}\omega + \boldsymbol{I}^{-1}(k_f H_t - k_t \boldsymbol{H}_f)\rho) \\ \boldsymbol{R}_b^e \boldsymbol{S}(\omega)\upsilon + \boldsymbol{R}_b^e(gH_g - \boldsymbol{S}(\omega)\upsilon + \frac{k_f}{M_{tot}}\boldsymbol{H}_f\rho) \end{bmatrix} \\ &= \begin{bmatrix} \left(\dot{\boldsymbol{\Psi}} - \boldsymbol{\Psi}\boldsymbol{I}^{-1}\boldsymbol{S}(\omega)\boldsymbol{I}\right)\omega \\ g\boldsymbol{R}_b^e H_g \end{bmatrix} + \begin{bmatrix} \boldsymbol{\Psi}\boldsymbol{I}^{-1}\left(k_f \boldsymbol{H}_t - k_t \boldsymbol{H}_f\right) \\ \frac{k_f}{M_{tot}}\boldsymbol{R}_b^e \boldsymbol{H}_f \end{bmatrix}\rho \end{aligned} \tag{32}$$

where

$$\dot{\boldsymbol{\Psi}} = \frac{\partial \boldsymbol{\Psi}}{\partial \phi_v}\dot{\phi}_v + \frac{\partial \boldsymbol{\Psi}}{\partial \theta_v}\dot{\theta}_v \tag{33}$$

and $\dot{\phi}_v$, $\dot{\theta}_v$ are obtained from Eq. (28) as: $\dot{\eta} = \boldsymbol{\Psi}\omega^b$.

We define the decoupling matrix $\boldsymbol{\beta}(x)$ as:

$$\boldsymbol{\beta}(x) = \begin{bmatrix} \boldsymbol{\Psi}\boldsymbol{I}^{-1}\left(k_f H_t - k_t \boldsymbol{H}_f\right) \\ \frac{k_f}{M_{tot}}\boldsymbol{R}_b^e \boldsymbol{H}_f \end{bmatrix} \tag{34}$$

We have $\det[\boldsymbol{\beta}(x)] \neq 0$ and the inverse $\boldsymbol{\beta}^{-1}(x)$ exists always[1] for all $x \in \mathbb{R}^{12}$ where x represents the states of the system. The relative degree of the system in the compact form is $r = r_1 + r_2 = 2+2 = 4$ which is equal to the number of states in the compact form of the dynamic equations, and there is no zero dynamics.

To linearize the system, we choose a new control input $\vartheta = \begin{bmatrix} \vartheta_1 \\ \vartheta_2 \end{bmatrix}$, and we write our desired linearized dynamics as: $y^{(2)} = \vartheta$.

From Eq. (32) we can write the feedback linearisation law as:

$$u = \boldsymbol{\beta}^{-1}\left(\vartheta - \begin{bmatrix} \left(\dot{\boldsymbol{\Psi}} - \boldsymbol{\Psi}\boldsymbol{I}^{-1}\boldsymbol{S}(\omega)\boldsymbol{I}\right)\omega \\ g\boldsymbol{R}_b^e H_g \end{bmatrix}\right). \tag{35}$$

The centralized input-output feedback linearization handles the coupling without the need for strict assumption on operating point to decouple the system. The linearized model in the compact form is given as:

$$\dot{\zeta} = \begin{bmatrix} 0 & 1 & 0 & 0 \\ 0 & 0 & 0 & 0 \\ 0 & 0 & 0 & 1 \\ 0 & 0 & 0 & 0 \end{bmatrix}\zeta + \begin{bmatrix} 0 & 0 \\ 1 & 0 \\ 0 & 0 \\ 0 & 1 \end{bmatrix}\vartheta \tag{36}$$

$$y = \begin{bmatrix} 1 & 0 & 0 & 0 \\ 0 & 0 & 1 & 0 \end{bmatrix}\zeta \tag{37}$$

where

$$\zeta = \begin{bmatrix} \eta \\ \dot{\eta} \\ \lambda \\ \dot{\lambda} \end{bmatrix} \in \mathbb{R}^{12},\ y = \begin{bmatrix} \eta \\ \lambda \end{bmatrix} \in \mathbb{R}^6,\ \vartheta = \begin{bmatrix} \vartheta_1 \\ \vartheta_2 \end{bmatrix} \in \mathbb{R}^6.$$

The linearized plant is a double integrator representing single degree of freedom for transitional and rotational motion.

[1]It is always assumed that $-\pi/2 < \theta_v < \pi/2$.

To control the linearized system, the $\mathscr{H}_\infty$ loop-shaping design is invoked to synthesize a controller for the linearized system. An algorithm proposed in [17] is invoked to simultaneously optimize the synthesis of loop-shaping weights and a stabilizing controller. This algorithm captures the design specification in a systematic manner while trying to maximize the robust stability margin of the closed-loop system. We fix the pre-compensator weight to a low-pass filter on all channels and use the algorithm to optimize an identical post-compensator weights for all channels. The optimized post-compensator for each channel is $w_2 = 105(s+0.6)/(s+8)^2$. The achieved robust stability margin is 0.51 which means a tolerance of approximately 51% of coprime factor uncertainty.

V. Simulation Results

To demonstrate numerical results, we simulate the Tri-rotor UAV along with the designed controller in Simulink. Figure 5 depicts the block digram for the simulation where $\begin{bmatrix} \eta_r & \lambda_r \end{bmatrix}^T$ is the desired reference attitude and position respectively.

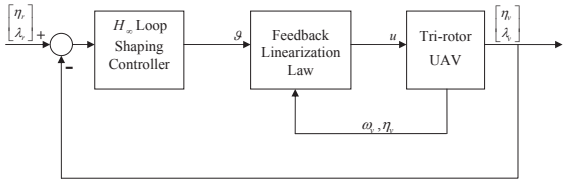

Figure 5. Simulation block diagram for the control design of the Tri-rotor UAV.

Figure 6 shows the singular values of the linearized plant, the shaped plant and the synthesized controller.

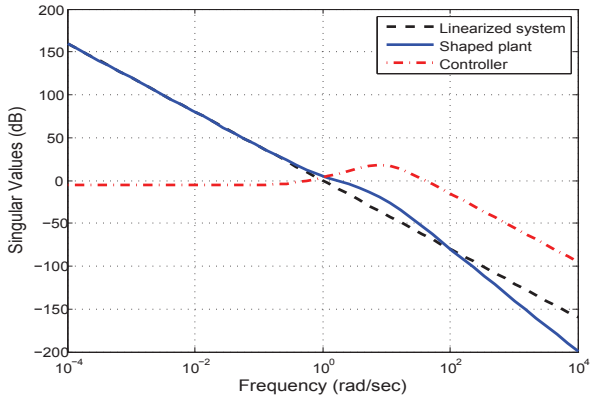

Figure 6. Singular value plots for the linearized system, the shaped system and the controller.

Figure 7 depicts the performance of the UAV for a scenario of horizontal hovering at height of 5 m where the vehicle was at a non-zero initial position and attitude as shown. The speed of the BLDC motors and the angles of the servo motors to stabilize the vehicle and track the references are shown in Figure 8. The controller shows good performance with tracking in all channels. The controller succeeds to maintain the stability of the vehicle and follow the reference trajectory for all initial conditions of the vehicle. The settling time

of the system is about 3 s which is acceptable taking into considering the slow dynamics of the vehicle. The servos and BLDC motors are not saturated and operate within their physical limits of $\pm 90^\circ$ for the servos and 12000 rpm for the BLDC motors, where these limits come from the technical specifications of the real actuators used in the Tri-rotor UAV.

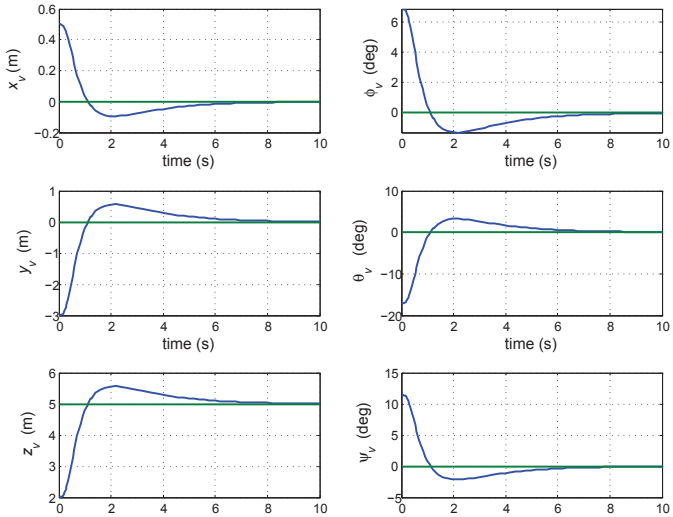

Figure 7. Simulation plots of the UAV position and attitude using the synthesized controller of $\mathscr{H}_\infty$ loop shaping control associated with classical feedback linearization.

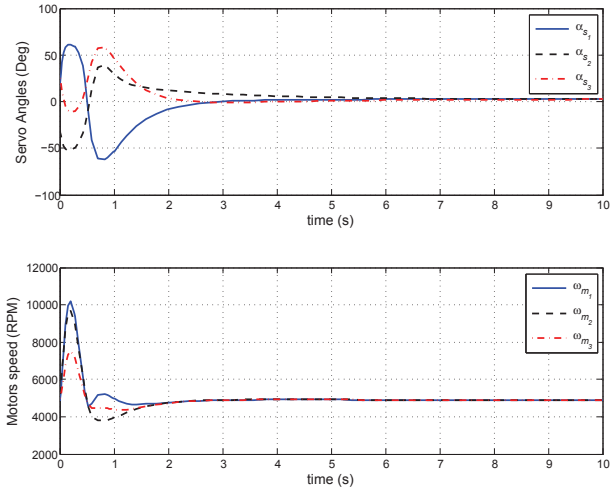

Figure 8. The performance of the actuators (servos and BLDC motors) to track the specified reference input of $(0,0,0)$ deg for attitude, and $(0,0,5)$ m for position coming from non-zero initial point.

VI. Conclusion

In this paper, a novel tri-rotor UAV is proposed. The proposed UAV has six actuators with full authority of thrust and torque vectoring. The mathematical model of the proposed design is non-linear and it indicates coupling between translational and rotational motion. The nonlinear model of the UAV is linearized by a centralized input-output feedback linearization. This procedure cancels the nonlinearity of all channels simultaneously without further conditions for specific operating point which is the case when we handle channels individually. The linearized plant is a double integrator that is controlled using $\mathscr{H}_\infty$ loop-design procedure. The result is verified via simulations. More complex feedback linearization techniques (such as robust feedback linearization in [18]) can be used in the same manner to avoid linearizing the system to a double integrator.

References

[1] A. Das, K. Subbarao, and F. lewis, "Dynamic inversion with zero-dynamics stabilisation for quadrotor contrl," *IET Control Theory and Applications*, vol. 3, pp. 303–314, 2009.

[2] K. P. Valavanis, Ed., *Advances in Unmanned Aerial Vehicles: State of the Art and the Road to Autonomy*, ser. International Series on Intelligent Systems, Control, and Automation: Science and Engineering. Springer, 2007, vol. 33.

[3] J. Escareno, A. Sanchez, O. Garcia, and R. Lozano, "Triple tilting rotor mini-UAV: Modeling and embedded control of the attitude," in *American Control Conference*, 2008, pp. 3476–3481.

[4] S. Salazar-Cruz, R. Lozano, and J. Escareño, "Stabilization and non-linear control for a novel trirotor mini-aircraft," *Control Engineering Practice*, vol. 17, no. 8, pp. 886–894, August 2009.

[5] R. Huang, Y. Liu, and J. J. Zhu, "Guidance, navigation, and control system design for tripropeller vertical-takeoff-and-landing unmanned air vehicle," *Journal of Aircraft*, vol. 46, no. 6, pp. 1837–1856, November-December 2009.

[6] D.-W. Yoo, H.-D. Oh, D.-Y. Won, and M.-J. Tahk, "Dynamic modeling and stabilization technique for tri-rotor unmanned aerial vehicles." *International Journal of Aeronautical and Space Science.*, vol. 11, pp. 167–174, 2010.

[7] P. Vanblyenburgh, "UAVs: An Overview," *Air & Space Europe*, vol. 1, no. 5-6, pp. 43–47, September 1999.

[8] B. Crowther, A. Lanzon, M. Maya-Gonzalez, and D. Langkamp, "Kinematic analysis and control design for a non planar multirotor vehicle," *Journal of Guidance, Control, and Dynamics*, vol. 34, no. 4, pp. 1157–1171, 2011.

[9] F. Lin, W. Zhang, and R. D. Brandt, "Robust hovering control of a PVTOL aircraft," *Control Systems Technology, IEEE Transactions on*, vol. 7, no. 3, pp. 343–351, August 2002.

[10] P. Rongier, E. Lavarec, and F. Pierrot, "Kinematic and dynamic modeling and control of a 3-rotor aircraft," in *Robotics and Automation, 2005. ICRA 2005. Proceedings of the 2005 IEEE International Conference on*, 2005, pp. 2606–2611. [Online]. Available: http://ieeexplore.ieee.org/xpls/abs_all.jsp?arnumber=1570506

[11] P. Fan, X. Wang, and K.-Y. Cai, "Design and control of a tri-rotor aircraft," in *Control and Automation (ICCA), 2010 8th IEEE International Conference on*, June 2010, pp. 1972 –1977.

[12] Z. Prime, J. Sherwood, M. Smith, and A. Stabile, "Remote control (rc) vertical take-off and landing (vtol) model aircraft," LevelIV Honours Project Final Report, University of Adelaide, Adelaide, Australia, October 2005.

[13] W. F. Phillips, *Mechanics of Flight*. Wiley & Sons, Inc., 2004.

[14] W. Z. Stepniewski and C. N. Keys, *Rotory-Wing Aerodynamics*. Dover Publications, Inc., 1984.

[15] G. D. Padfield, *Helicopter Flight Dynamics: The Theory and Application of Flying Qualities and Simulation Modeling*, ser. Education Series. AIAA, 1996.

[16] A. Isidori, L. Marconi, and A. Serrani, *Robust Autonomous Guidance: An Internal Model Approach*, 1st ed., ser. Advanced in Industrial Control. Springer, 2003.

[17] A. Lanzon, "Weight optimisation in H_∞ loop-shaping," *Automatica*, vol. 41, no. 7, pp. 1201–1208, 2005.

[18] A. L. D. Franco, H. Bourlès, E. R. De-Pieri, and H. Guillard, "Robust nonlinear control associating robust feedback linearization and H_∞ control," *IEEE Transactions on Automatic Control*, vol. 51, no. 7, pp. 1200–1206, 2006.